Enhanced Digital PI Control with State-Variable Feedback Loop for DC Electric Springs

Yun Yang*, Siew-Chong Tan*
*Department of Electrical and Electronic Engineering
The University of Hong Kong, Hong Kong
Email: sctan@eee.hku.hk

Shu-Yuen (Ron) Hui*†
†Department of Electrical and Electronic Engineering
Imperial College London, U.K.
Email: ronhui@eee.hku.hk

***Abstract*—DC electric springs (DCES) have recently been proposed as a potential solution for resolving the issue of power supply-demand imbalance of DC microgrids caused by the fluctuations of intermittent renewable energy sources (RES). Existing control of DCES based on conventional PI compensation are designed for good steady-state performance. The dynamic performance of DCES is typically neglected. In this paper, an enhanced digital PI control comprising a state-variable feedback loop, aimed at optimizing both the steady-state and transient performances of the DCES, is proposed. Experiment results show that with this control, faster transient of the DCES is achievable and that the DCES can rapidly tame the possible fluctuations of renewable energy sources in a 48 V DC test grid more effectively.**

Keywords—DC microgrids, DC electric springs (DCES), dynamic modeling, digital feedback control, state-variable feedback.

I. INTRODUCTION

At power distribution and utilization levels, DC microgrids possess advantages such as high efficiency, high reliability, and easy interconnection of renewable sources as compared to AC microgrids [1]−[4]. This is possible as most microgrid facilities comprising photovoltaic (PV) systems, fuel cells, batteries, and major customer's loads are inherently of DC nature, and that DC/AC (reciprocally AC/DC) conversions can be avoided to improve the energy transfer process [5]. DC microgrids are still primarily at test-platform stages globally, but their wide applications are expected in the near future. Before this is possible, several issues pertaining to the DC microgrid technology (such as protection and stability) must be resolved.

One critical issue (the crux of this research work) is that a high penetration of renewable energy sources can easily induce unstable phenomenon in the DC microgrids. To resolve such an issue, demand-side management (DSM) is primarily adopted [6]−[8]. DSM comprises a portfolio of measures that improve the supply-demand balancing of the power system on the utility consumption side. With DSM, the electricity demand and supply are brought closer to a perceived optimum range with regards to improving energy efficiency, and may involve sophisticated real-time control of distributed energy resources [9]. Smart loads play important roles in DSM. The DC electric springs (DCES), which is derived from the concepts of AC electric springs [10]−[22], is a kind of smart load that has been proposed for mitigating the effect of voltage fluctuations in DC microgrids [23]−[25].

So far, it has been demonstrated that DCES can be applied for bus voltage regulation, harmonics mitigations, fault-ride-through support, power supply and demand balancing, and reducing energy storage requirement of DC microgrids [23], [24]. As investigations are still preliminary, the control strategies presented for the DCES are mainly concerned with their steady-state performances [23]−[25]. Clearly, a DCES with better dynamic performance can greatly improve the quality of protection of the critical loads and reduce the redundant energy loss of the microgrid.

In this paper, an enhanced digital proportional-integral (PI) control strategy involving a state-variable feedback loop for improving both steady-state and transient performance, is proposed. This control is based on a dynamic model of the DCES that is described in this paper. To validate the utility of the DCES in achieving rapid mitigation of the renewable energy source variation, experiment involving a full-bridge inverter as DCES, is conducted on a 48 V DC test grid.

II. SMALL-SIGNAL DYNAMIC MODEL OF DCES

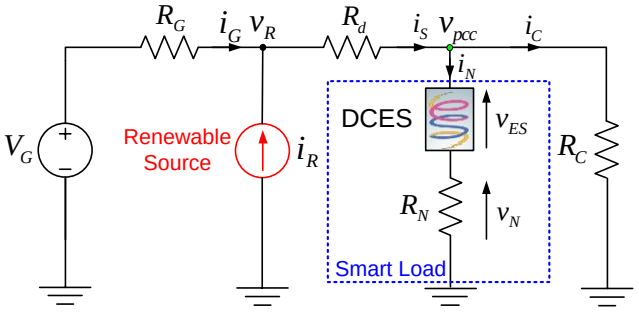

Fig. 1. Simplified diagram of a DC microgrid with a DCES.

A simplified diagram of a DC microgrid with an installed ES can be depicted as shown in Fig. 1. Here, V_G is a constant DC voltage source; R_G is the internal resistance of V_G; i_R is the time-varying current injected by the renewable energy source; R_d is the resistance of the distributed line; R_C is the critical load

(voltage sensitive equipment), which requires a well-regulated mains voltage; R_N is the non-critical load representing appliances that can tolerate a wider range of voltage and power fluctuation. The DCES can be operated such that the power consumption of R_N follows the variation of the renewable power generation. In doing so, the DCES reform the non-critical loads into smart loads, which adaptively regulate the point-of-common-coupling (PCC) voltage v_{pcc} to accommodate the specifications of critical loads.

Based on Norton's theorem, the equivalent model of the microgrid with DCES shown in Fig. 1 can be depicted as shown in Fig. 2, where d is the duty ratio and $v_a(d,V_{dc})$ is the output voltage of the controllable voltage source, which is correlated to d and the voltage source of DCES V_{dc}.

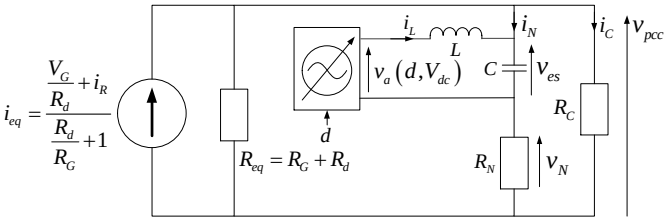

Fig. 2. Equivalent model of a DC microgrid with DCES.

From Fig. 2, the state-space averaged model equation of the DCES can be derived as

$$\begin{cases} \dfrac{di_L}{dt} = -\dfrac{v_{es}}{L} + \dfrac{v_a}{L} \\ \dfrac{dv_{es}}{dt} = \dfrac{i_L}{C} + \dfrac{i_N}{C} \end{cases}, \tag{1}$$

where L and C are the inductor and capacitor of the DCES, i_L is the current of the inductor, v_{es} is the output voltage of the DCES, and i_N is the current of the non-critical load.

The corresponding small-signal model equation in the Laplace domain can be obtained from (1) as

$$\begin{cases} \tilde{v}_a(s) = sL\tilde{i}_L(s) + \tilde{v}_{es}(s) \\ \tilde{i}_N(s) = -\tilde{i}_L(s) + sC\tilde{v}_{es}(s) \end{cases}, \tag{2}$$

where $\tilde{v}_a(s)$, $\tilde{i}_N(s)$, $\tilde{i}_L(s)$ and $\tilde{v}_{es}(s)$ are small-signal AC values of $v_a(s)$, $i_N(s)$, $i_L(s)$, and $v_{es}(s)$, respectively. Equation (2) can be pictorially described as shown in Fig. 3.

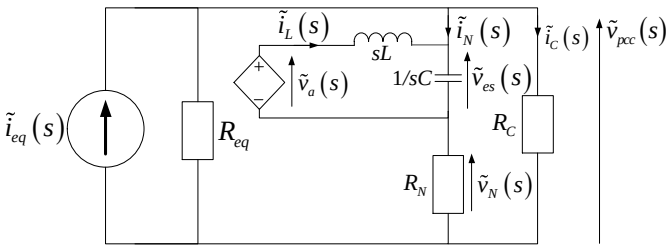

Fig. 3. Small-signal model of a DC microgrid with DCES.

Apparently, the small-signal dynamic model equation of the DCES can be written as

$$\tilde{v}_{es}(s) = \frac{1}{1+LCs^2}\tilde{v}_a(s) + \frac{Ls}{1+LCs^2}\tilde{i}_N(s), \tag{3}$$

and the small-signal equation of the PCC voltage $\tilde{v}_{pcc}(s)$ will be

$$\tilde{v}_{pcc}(s) = \frac{1}{1+LCs^2}\tilde{v}_a(s) + \frac{LCR_Ns^2 + Ls + R_N}{1+LCs^2}\tilde{i}_N(s). \tag{4}$$

III. Digital PI Control with State-Variable Feedback Loop of DCES

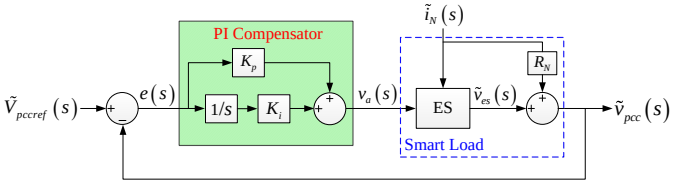

Fig. 4. Typical PI control block diagram of DCES.

Fig. 4 shows the small-signal Laplace representation of the control block diagram of a typical PI controller used in DCES. Here, $\tilde{V}_{pccref}(s)$ is the small-signal value of the reference of the PCC voltage. Based on (4), the closed-loop transfer function of $\tilde{v}_{pcc}(s)$ and $\tilde{V}_{pccref}(s)$ and that of $\tilde{v}_{pcc}(s)$ and $\tilde{i}_N(s)$ of the DCES under this control can be given as

$$G_{TT1}(s) = \frac{\tilde{v}_{pcc}(s)}{\tilde{V}_{pccref}(s)} = \frac{K_p s + K_i}{LCs^3 + (K_p + 1)s + K_i}, \tag{5}$$

$$G_{TT2}(s) = \frac{\tilde{v}_{pcc}(s)}{\tilde{i}_N(s)} = \frac{R_N LCs^3 + Ls^2 + R_N s}{LCs^3 + (K_p + 1)s + K_i}, \tag{6}$$

where K_p and K_i are the tuning coefficients of the proportional and integral terms of the PI controller. This controller can be easily implemented in analog or digital form to fulfill the requirement of the steady-state performance of the DC microgrid. However, a fast dynamic performance of the DCES in dealing with disturbances and a fluctuating renewable energy source cannot be easily achieved with this controller.

To resolve this issue, the PI controller described above is modified to include a state-variable feedback loop. This enables the system poles to be freely altered to satisfy a certain dynamic performance of the DCES. Fig. 5 shows the proposed control, where K_1 and K_2 are the coefficients for setting the location of poles in the complex plane. The state-variable feedback loop involves the state variables $V_{pcc}(s)$ and $i_N(s)$. The number of state variables corresponds to the number of roots of the characteristic equation. The location of the eigenvalue can be selected through the choice of K_1 and K_2.

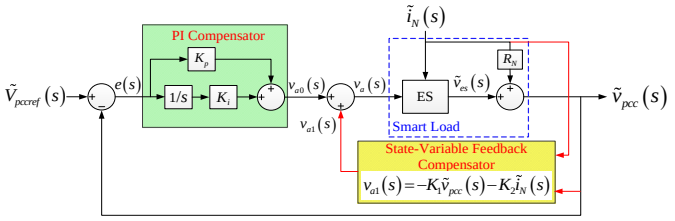

Fig. 5. Block diagram of the proposed enhanced digital PI control with state-variable feedback loop.

The transfer function describing the closed-loop relationship of the DCES under the proposed control can be expressed as

$$G_{TP1}(s)=\frac{\tilde{v}_{pcc}(s)}{\tilde{V}_{pccref}(s)}=\frac{K_p s+K_i}{LCs^3+(K_p-K_1+1)s+K_i}, \quad (7)$$

$$G_{TP2}(s)=\frac{\tilde{v}_{pcc}(s)}{\tilde{i}_N(s)}=\frac{R_N LCs^3+Ls^2+(R_N-K_2)s}{LCs^3+(K_p-K_1+1)s+K_i}. \quad (8)$$

By reorganizing and combining (7) and (8), it is possible to derive the transfer function as

$$\begin{aligned}\tilde{v}_{pcc}(s)=&\frac{(\tilde{V}_{pccref}(s)-\tilde{v}_{pcc}(s))\left(\frac{K_i}{s}\right)}{1+LCs^2}+\frac{K_p\tilde{V}_{pccref}(s)}{1+LCs^2}\\&+\frac{-(K_1+K_p)\tilde{v}_{pcc}(s)-K_2\tilde{i}_N(s)}{1+LCs^2}\\&+\frac{LCR_Ns^2+Ls+R_N}{1+LCs^2}\tilde{i}_N(s).\end{aligned} \quad (9)$$

Apparently, the first term $\frac{(\tilde{V}_{pccref}(s)-\tilde{v}_{pcc}(s))\left(\frac{K_i}{s}\right)}{1+LCs^2}$ has the function of eliminating the steady-state error (since there is a pole at origin in the numerator) when the system's parameters vary. However, the presence of this pole will introduce a –90° phase shift into the system, which reduces the phase margin of the system. This in turns limits the allowable bandwidth of the controller [26]. The second derived term $\frac{K_p\tilde{V}_{pccref}(s)}{1+LCs^2}$ is a resulting feedforward term of the control in dealing with a fast change of the reference of the PCC voltage. The third term $\frac{-(K_1+K_p)\tilde{v}_{pcc}(s)-K_2\tilde{i}_N(s)}{1+LCs^2}$ is the state-variable feedback term, which influences the dynamic performance of the system via the choice of K_1 and K_2. The fourth term $\frac{LCR_Ns^2+Ls+R_N}{1+LCs^2}\tilde{i}_N(s)$ gives the mathematical description of the smart load system. The determination of K_1 and K_2 is not straightforward. The control input $v_{a1}(s)$ resulted from the state-variable feedback loop as shown in Fig. 5, is a linear combination of the state variables and is given by

$$v_{a1}(s)=-K_{I1}\tilde{i}_L(s)-K_{V1}\tilde{v}_{es}(s). \quad (10)$$

where K_{I1} and K_{V1} are the feedback coefficients of $\tilde{i}_L(s)$ and $\tilde{v}_{es}(s)$, respectively. Besides, $\tilde{i}_N(s)$ can also be given by the linear combination of the state variables as

$$\tilde{i}_N(s)=-K_{I2}\tilde{i}_L(s)-K_{V2}\tilde{v}_{es}(s). \quad (11)$$

Then, it can be derived that

$$v_{a1}(s)=-\begin{bmatrix}K_1 & K_2\end{bmatrix}\begin{bmatrix}\tilde{v}_{pcc}(s)\\ \tilde{i}_N(s)\end{bmatrix}, \quad (12)$$

where

$$K_1=\frac{K_{V1}K_{I2}-K_{V2}K_{I1}}{K_{I2}}-K_p, \quad (13)$$

$$K_2=\frac{K_{V2}K_{I1}R_N-K_{V1}K_{I2}R_N-K_{I1}}{K_{I2}}. \quad (14)$$

The values of K_{I1}, K_{V1}, K_{I1} and K_{V1} can be obtained by using ***acker*** function in MATLAB/SIMULINK, such that

$$\begin{bmatrix}K_{I1} & K_{V1}\end{bmatrix}=\textbf{\textit{acker}}\left(\begin{bmatrix}0 & -\frac{1}{L}\\ \frac{1}{C} & 0\end{bmatrix},\begin{bmatrix}\frac{1}{L}\\ 0\end{bmatrix},\mathbf{P_d}\right), \quad (15)$$

$$\begin{bmatrix}K_{I2} & K_{V2}\end{bmatrix}=\textbf{\textit{acker}}\left(\begin{bmatrix}0 & -\frac{1}{L}\\ \frac{1}{C} & 0\end{bmatrix},\begin{bmatrix}0\\ \frac{1}{C}\end{bmatrix},\mathbf{P_d}\right), \quad (16)$$

where $\mathbf{P_d}$ is the desired location of poles in the complex plane. By substituting (15) and (16) into (13) and (14), K_1 and K_2 can be obtained.

IV. Simulation Results

The simulation is conducted based on the parameters given in Table I using MATLAB/SIMULINK. By designating the desired poles as $\mathbf{P_d}=[-10+5i \quad -10-5i]$, the values of $[K_{I1} \quad K_{V1}]$ and $[K_{I2} \quad K_{V2}]$ can be obtained using (15) and (16). The code in MATLAB is given below.

```
Pd=[-10+5*i -10-5*i];
F=[0 -2000;75757.58 0];
G1=[2000;0];
G2=[0;75757.58];
Ku=acker(F,G1,Pd)
Kc=acker(F,G2,Pd)
```

TABLE I. SPECIFICATIONS OF SMART LOAD AND RENEWABLE SOURCE

Description	Parameter	Value
Nominal DC bus voltage	V_{pcc_nom}	48 V
Distribution line resistance	R_d	2.5 Ω
Critical load resistance	R_C	50 Ω
Noncritical load resistance	R_N	50 Ω
Rated DCES minimum voltage	V_{es_min}	−60 V
Rated DCES maximum voltage	V_{es_max}	60 V
Rated smart load minimum current	I_{N_min}	−12 A
Rated smart load maximum current	I_{N_max}	12 A
Inductance of DCES output filter	L	500 μH
Capacitance of DCES output filter	C	13.2 μF

Under the given parameters, the computed results are K_{I1}=0.01, K_{V1}=−1, K_{I2}=1 and K_{V2}=0.0003. With that, K_1 and K_2 can be derived based on (13) and (14) as K_1=−1.05 and K_2=49.99. Fig. 6 shows the Bode plots of the closed-loop system of the DCES with both the conventional PI control and the proposed PI control with state-variable feedback loop, under the same PI setting of K_p=0.05 and K_i=15.

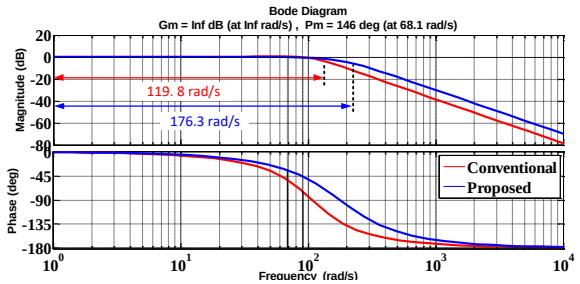

Fig. 6. Bode plots of the closed-loop system with the conventional PI control and the proposed PI control with state-variable feedback loop.

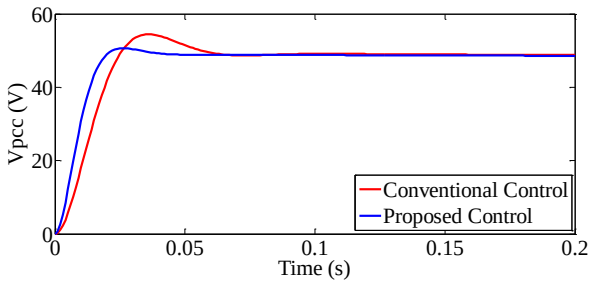

Fig. 7. Waveform of the common-coupling-point voltage of the closed-loop system with both the conventional PI control and the proposed PI control with state-variable feedback loop.

Apparently, the closed-loop system with the proposed control method has a wider bandwidth of 176.3 rad/s than that of the conventional PI control 119.8 rad/s (47.16% improvement), which means that the system is inherently of a faster dynamic response under the same PI control setting. The comparison of the corresponding waveforms of v_{pcc} between the two control schemes is provided in Fig. 7. Clearly, the system with the proposed control achieves a better dynamic performance in terms of a shorter settling time and smaller overshoot.

V. EXPERIMENTAL VERIFICATION

The experiment is conducted on a DC microgrid with a nominal V_{pcc} of 48 V. The DCES is implemented using a full-bridge inverter that is controlled by a digital signal processor (DSP) TMS320F28069 (Texas Instruments Inc.). A simplified schematic diagram of the experiment setup is given in Fig. 8 (relays and sensors are not presented). The renewable source is emulated by a programmable voltage source PCR2000LE (Kikusui Inc.). The specifications of the main components are provided in Table I. The schematic block diagram of the control algorithm that is programmed into the DSP is shown in Fig. 9.

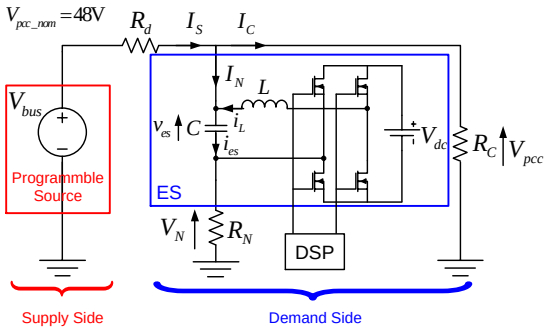

Fig. 8. Simplified schematic diagram of the experiment setup.

Fig. 10 shows the experiment waveforms of V_{bus}, V_{pcc}, and V_{es} of the system before and after the activation of DCES in achieving PCC voltage regulation. The renewable energy source is operated at V_{bus} = 51.5 V. It is shown that there is a noticeable change of V_{pcc} from 46.8 V to the nominal value of 48 V when the non-critical load is converted into a smart load through the activation of ES. It illustrates that the proposed enhanced digital PI control with state-variable loop can achieve the required PCC regulation.

To study the performance of the DCES under the proposed control in stabilizing the DC microgrid during renewable fluctuations, an experiment with fluctuating voltage source is performed over a period of time, of which the measured data of V_{pcc} and V_{es} are stored and then plotted via MATLAB. Fig. 11 shows the experiment waveforms of V_{pcc} and V_{es} of the system for a time frame of 50 seconds. From 0 to 5 s, the renewable energy source is programmed to contain no fluctuation such that V_{pcc} is 48 V and that DCES is deactivated. From 5 to 25 s, the renewable energy source is programmed to contain variations that changes at 1 *s* sampling time within the range of 5% (V_{pcc} randomly varies within 45.6 to 50.4 V) and that DCES is still deactivated. From 25 to 50 *s*, the random variation of V_{pcc} is still present, but the DCES is activated. As shown in Fig. 11, with the DCES turned on, V_{pcc} is well-regulated at steady state voltage 48 V despite the variation of the renewable.

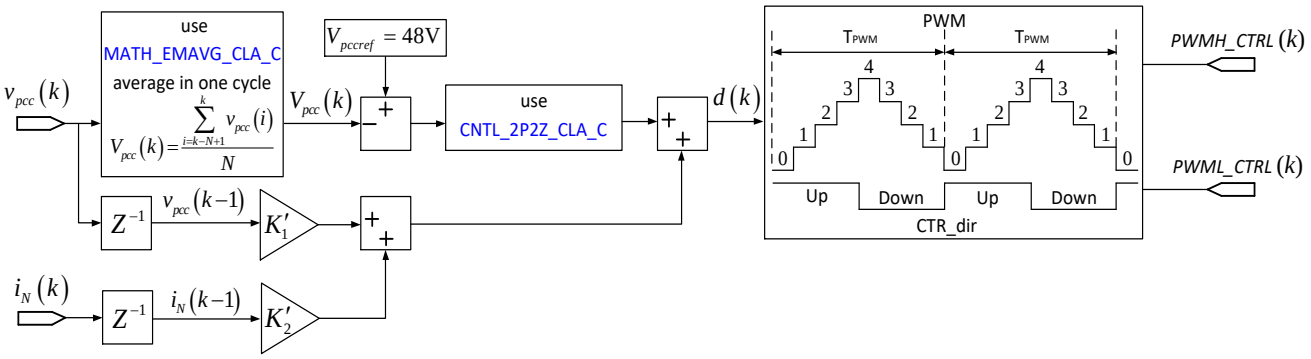

Fig. 9. Schematic block diagram of the control algorithm programmed into the DSP.

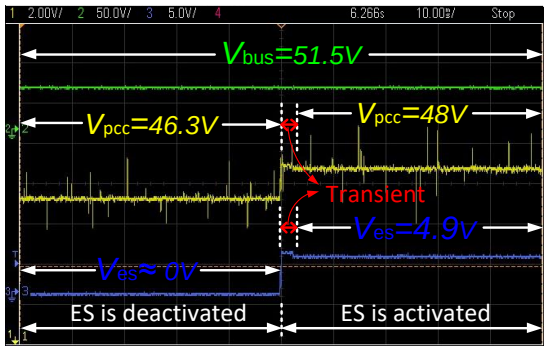

Fig. 10. Experiment waveforms of V_{bus}, V_{pcc}, and V_{es} before and after the activation of DCES.

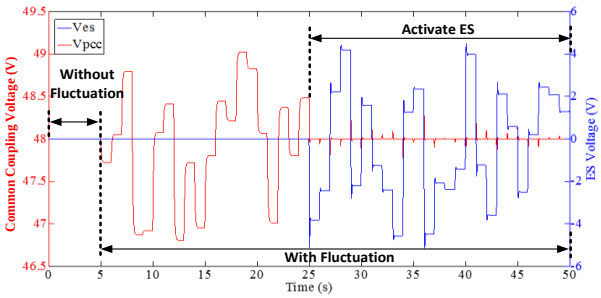

Fig. 11. Experiment waveforms of V_{pcc} and V_{es} of the system operating with renewable source with/without fluctuation and the DCES deactivated/activated.

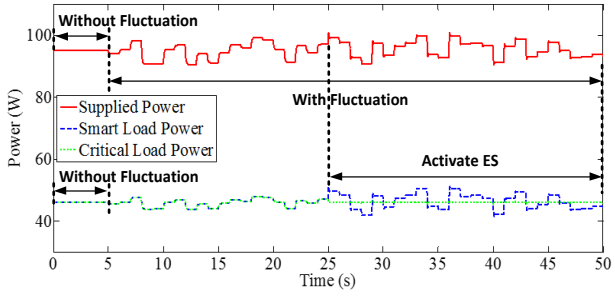

Fig. 12. Experiment waveforms of the supplied power, smart-load power, and critical-load power of the system operating with the renewable source with/without fluctuation and the DCES deactivated/activated.

Fig. 12 shows the corresponding experiment waveforms of the supplied power, the smart-load power, and the critical-load power of the system over the same timeframe. Before activating the DCES, both the critical and non-critical loads consume the same supplied power, and that the critical-load power fluctuates correspondingly. However, after the DCES is being activated, the critical-load power is regulated steadily at 48 W consumption. The fluctuation portion of the supplied power is fully absorbed by the smart load. A dynamic comparison of the waveform of V_{pcc} between the use of conventional PI control and that of the proposed PI control with state-variable feedback loop, when the source voltage V_{bus} changes from 51.5 V to 54.0 V, is given in Fig. 13. Apparently, the dynamic performance is very much improved with the proposed PI control.

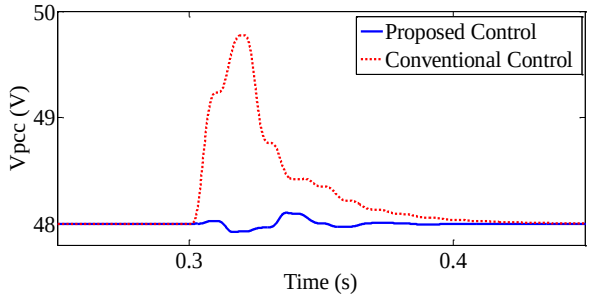

Fig. 13. Experiment waveforms of V_{pcc} of the system during transient. The DCES operates under conventional PI control and the proposed PI control with feedback loop.

VI. CONCLUSIONS

Existing proportional-integral (PI) control of DCES, which has been well-validated to ensure the steady-state performance of DC microgrids, are found to be inadequate in addressing applications with fast dynamic requirement. An enhanced digital proportional-integral (PI) control comprising a state-variable feedback loop based for improving both the dynamic and steady-state performances of the DCES, is proposed. Discussions on its theoretical derivation and design have been covered. From the simulations results, it is shown that the addition of the state-variable feedback loop to the PI control

has increased the bandwidth of the system by about 47.16%, thereby leading to a faster dynamic response. This is verified experimentally. Moreover, the experimental results also show that the proposed enhanced digital PI control with state-variable loop can easily achieve the required PCC regulation.

ACKNOWLEDGMENT

This project is supported in part by the Hong Kong Research Grant Council under the Theme-Based Research Scheme T23-701/14-N.

REFERENCES

[1] B. C. Beaudreau, *World Trade: A Network Approach*, iUniverse, 2004.

[2] G. Neidhofer, "Early three-phase power," *Power and Energy Magazine IEEE*, vol. 5, no. 5, pp.88-100, Sep. 2007.

[3] R. H. Lasseter and P. Paigi, "Microgrid: a conceptual solution," in *Proc. IEEE Power Electron. Spec. Conf.*, 2004, pp. 4285-4290.

[4] S. Anand, B. G. Fernandes, and J. M. Guerrero, "Distributed control to ensure proportional load sharing and improve voltage regulation in low-voltage dc microgrids," *IEEE Tran. Power Electron.*, vol. 28, no. 4, pp. 1900-1913, Aug. 2012.

[5] P. Loh, D. Li, Y. K. Chai, and F. Blaabjerg, "Autonomous operation of hybrid microgrid with AC and DC subgrids," *IEEE Tran. Power Electron.*, vol. 28, no. 5, pp. 2214-2223, May 2013.

[6] N. Eghtedarpou and E. Farjah, "Power control and management in a hybrid AC/DC microgrid," *IEEE Trans. Smart Grid*, vol. 5, no. 3, pp. 1494-1505, May 2014.

[7] N. Kinhekar, N. P. Pardhy, F. Li, and H. O. Gupta, "Utility oriented demand side management using smart AC and micro DC grid cooperative," *IEEE Trans. Power Syst.*, vol. 31, no. 2, pp. 1151-1160, Mar. 2016.

[8] Y. K. Tan, T. P. Huynh, and Z. Wang, "Smart personal sensor network control for energy saving in DC grid powered LED lighting system," *IEEE Trans. Smart Grid*, vol. 4, no. 2, pp. 669-676, Jun. 2013.

[9] P. Palensky and D. Dietrich, "Demand side management: demand response, intellgent energy systems, and smart loads," *IEEE Trans. Ind. Informat.*, vol. 7, no. 3, pp. 381-388, Jun. 2011.

[10] S. Y. R. Hui, C. K. Lee, and F. F. Wu, "Electric springs-A new smart grid technology," *IEEE Trans. Smart Grid*, vol. 3, no. 3, pp. 1552-1561, Sept. 2012.

[11] N. R. Chaudhuri, C. K. Lee, B. Chaudhuri, and S. Y. R. Hui, "Dynamic modeling of electric springs," *IEEE Trans. Smart Grid*, vol. 5, no. 5, pp. 2450-2458, Sept. 2013.

[12] C. K. Lee and S. Y. R. Hui, "Reduction of energy storage requirements in future smart grid using electric springs," *IEEE Trans. Smart Grid*, vol. 4, no. 3, pp. 1282-1288, Sept. 2013.

[13] S. C. Tan, C. K. Lee, and S. Y. R. Hui, "General steady-state analysis and control principle of electric springs with active and reactive compensations," *IEEE Trans. Power Electron.*, vol. 28, no. 8, pp. 3958-3969, Aug. 2013.

[14] X. Luo, Z. Akhtar, C. K. Lee, B. Chaudhuri, S. C. Tan, and S. Y. R. Hui, "Distributed voltage control with electric springs: Comparisons with STATCOM," *IEEE Trans. Smart Grid*, vol. 6, no. 1, pp. 209-219, Jan. 2015.

[15] K. T. Mok, S. C. Tan, and S. Y. R. Hui, "Decoupled power angle and voltage control of electric springs," *IEEE Trans. Power Electron.*, vol. 31, no. 2, Feb. 2016.

[16] X. Chen, Y. Hou, S. C. Tan, C. K. Lee, and S. Y. R. Hui, "Mitigating voltage and frequency fluctuation in microgrids using electric springs," *IEEE Trans. Smart Grid*, vol. 6, no. 2, pp. 508-515, Mar. 2015.

[17] J. Soni, K. R. Krishnanand, and S. K. Panda, "Load-side demand management in buildings using controlled electric springs," in *Ind. Electron. Society, IECON 2014*, Oct. 2014, pp. 5376–5381.

[18] Q. Wang, M. Cheng, Z. Chen, and Z. Wang, "Steady-state analysis of electric springs with a novel δ control," *IEEE Trans. Power Electron.*, vol. 30, no. 12, Jan. 2015.

[19] S. Yan, S. C. Tan, C. K. Lee, B. Chaudhuri, and S. Y. Hui, "Electric spring for reducing power imbalance in three-phase power systems," *IEEE Trans. Power Electron.*, vol. 30, no. 7, pp. 3601-3609, Aug. 2014.

[20] K. R. Krishnanand, S. M. F. Hasani, J. Soni, and S. K. Panda, "Neutral current mitigation using controlled electric springs connected to microgrids within build environment," in *Proc. IEEE Energy Convers. Congr. Expo.*, Sep. 2014, pp. 2947–2951.

[21] Y. Yang, S. C. Tan, and S. Y. R. Hui, "Voltage and frequency control of electric spring based smart loads," in *IEEE Applied Power Electron. Confer. Expo. (APEC)*, 2016, pp. 3481–3487.

[22] Y. Yang, S. S. Ho, S. C. Tan, and S. Y. R. Hui, "Small-signal model and stability of electric springs in power grids," *IEEE Trans. Smart Grid*, vol. PP, no. 99, pp. 1-1, Mar. 2016.

[23] M. H. Wang, K. T. Mok, S. C. Tan, and S. Y. R. Hui, "Multifunctional DC electric springs for improving voltage quality of DC grids," *IEEE Tran. Smart Grid*, vol. PP, no. 99, pp. 1-1, Jan. 2016.

[24] M. H. Wang, S. C. Tan, and S. Y. R. Hui, "Reduction of storage capacity in DC microgrids using PV-embedded series DC electric springs," in *IEEE Applied Power Electron. Conf. Expo. (APEC)*, 2016, pp. 3302-3309.

[25] Q. S. Wang, M. Cheng, et.al., "DC electric spring with DC/DC converters," in *IEEE 8th Int. Power Electron. Motion Control Conf.*, 2016, pp. 3268-3273.

[26] K. Ogata, *Modern Control Engineering*, NJ : Prentice Hall, 2010.